



## Research article

# Finite element simulation of the complete sheet metal blanking cycle: Effect of blanking clearance on force curve and cut edge quality

Jean Rizk <sup>a,b,\*</sup>, Mohamed Rachik <sup>a</sup>, Andre Maillard <sup>b</sup>

<sup>a</sup> Compiègne University of Technology, Roberval (Mechanics, Energy and Electricity), 60203, Compiègne, Cedex, France

<sup>b</sup> CETIM, Sheet Metals Unit, BP 80067, 60304, Senlis, Cedex, France

## ARTICLE INFO

**Keywords:**

Blanking operation  
Blanking force curve  
Cut edge quality  
Numerical simulation  
Finite element method

## ABSTRACT

Sheet metal blanking process is a manufacturing process that is widely used in sheet metal forming and particularly in the electronics and automotive industries. The outcome and quality of the blanked parts are affected by various parameters such as the blanking clearance, the sheet metal mechanical properties and the wear of tools. However, experimental campaigns to assess the effects of these parameters on the process outcome can be prohibitively expensive for the industry. As a result, numerical simulation of the blanking process is becoming increasingly important to gain insight into the process and study these effects.

The present paper provides a novel finite element (FE) simulation procedure to predict the complete blanking cycle including sheet metal cutting, sheet metal springback, punch penetration in die, and stripping phases. A blanking force curve showing the punch force at all phases can thus be obtained. The commercial finite element code ABAQUS® has been chosen to develop this procedure using ABAQUS/Explicit® code for the cutting phase and ABAQUS/Standard® code for the remaining phases. Based on this procedure, the influence of the blanking clearance on the punch force-displacement curve and on the cut edge quality has been studied. The obtained results have been compared to previous literature results and experimental findings.

## 1. Introduction

Sheet metal blanking is one of the most widely used manufacturing processes in several industries. While its application ranges from small electronics components to heavy automotive parts, this process is well known for its reliability in mass production industries and for its high productivity rate.

A blanking operation is accomplished by a shearing action on a thin plate placed between a fixed die and a moving punch. The primary objective of such processes is to separate the sheet by leading it to plastic shearing followed by a crack initiation and propagation. Fig. 1 shows a schematic description of a blanking tool.

The blanking process is primarily monitored using the blanking force signal, which measures the force on the punch during its travel. The blanking force is the most informative signal in blanking as it provides valuable insights into the detailed mechanism of the process. Recently, this signal has become more important due to its use in monitoring the punch wear. The punch wear is a critical issue

\* Corresponding author. Compiègne University of Technology, Roberval (Mechanics, energy and electricity), 60203 Compiègne, Cedex, France.  
E-mail address: [jean.rizk@utc.fr](mailto:jean.rizk@utc.fr) (J. Rizk).

in blanking operations that can result in significant downtimes for the press machine. Recent investigations, such as the work of Bergs et al. [1] and Kubik et al. [2], have shown that the blanking force signal can be correlated to the punch wear. Other works, such as the work of Kubik et al. [3] and Niemietz et al. [4], have suggested artificial intelligence-based techniques to indirectly monitor the punch wear based on the force signal. Fig. 2 shows a typical blanking force curve as a function of the punch displacement. Based on this curve, a blanking operation can be divided into three major phases (Fig. 2):

- The cutting phase (also denoted as the punching phase) is when the punch begins its penetration until the sheet separation.
- The punch penetration in die phase (also denoted as the push phase) is when the punch penetrates in the die to push the cut blank outside of it.
- The stripping phase (also denoted as the withdraw phase) is when the punch is withdrawn from the die, indicating the end of the blanking operation.

The blanking force curve and the quality of the cut edge (Fig. 3) in a blanking process depend on various process parameters, such as the radial blanking clearance between the punch and the die, the geometries of the tools (primarily the cutting-edge radii), the use of lubrication, and the material's thickness. Many studies have investigated the effect of these parameters on the blanking process outcome. Of all the parameters, the radial blanking clearance is the most crucial and significant in blanking. Fang et al. [5] conducted a numerical study to investigate the effect of the blanking clearance on the blanking force curve and the cut edge profile. Their study showed that a smaller clearance results in higher punch forces and better cut edge quality. Hamblin [6] carried out a finite element numerical study to explore the effect of punch wear on the blanking force curve. The punch wear was simulated by increasing the punch cutting edge radius, and the author concluded that the blanking force increases as the punch wear increases. Other studies have examined the impact of various process parameters on the cut edge quality, including those reported by Husson et al. [7], Totre et al. [8], and Maiti et al. [9].

In recent years, advancements in computational capabilities have led to the development of numerous finite element studies to model the blanking process with applications spanning various domains. Husson et al. [7] studied the effect of various blanking parameters on the cut edge quality using a finite element simulation approach. Falconnet et al. [10] combined a finite element simulation model with an Archard wear algorithm to predict the wear of the cutting punch after one blanking operation. Sahli et al. [11] simulated a fine blanking operation using LS-Dyna® commercial code to study the effect of punch die clearance on the shear stress and plastic strain distribution in the shearing zone. Pathak et al. [12] investigated meso-scale punching of complex shapes in sheet metal. They developed a 2D finite element model for blanking simulation to assess the potential of blanking processes surpassing conventional silicon-based lithography processing techniques. Liu et al. [13] efficiently used finite element numerical simulation to explore the impacts of varying grain sizes on the results of fine micro-blanking processes. Predicting sheet metal separation requires the use of a numerical ductile fracture criterion. Various fracture criteria and damage models have been developed years ago, and many of them have been implemented in different finite element codes, such as ABAQUS/Explicit® and LS-Dyna®. These fracture criteria are typically classified into two groups: coupled models and uncoupled models. Coupled models, such as Lemaitre [14] and Gurson [15]

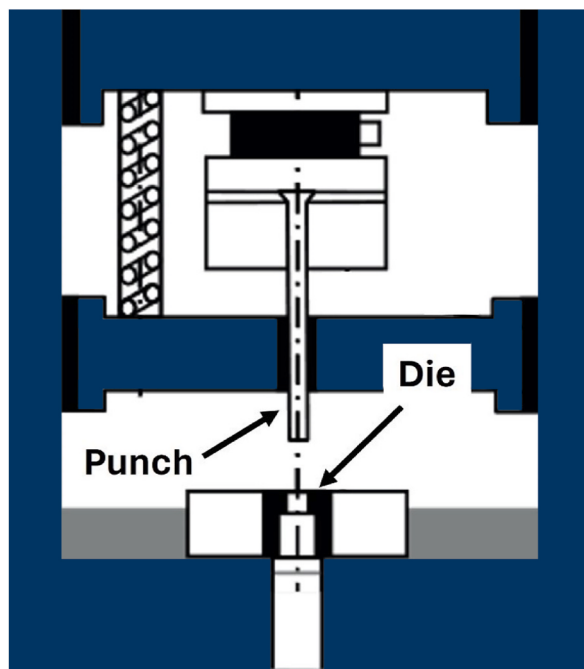


Fig. 1. Schematic description of a blanking tool.

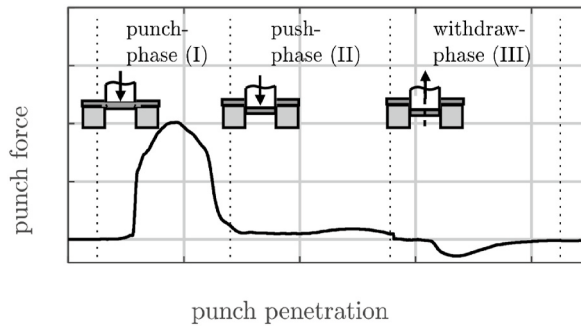


Fig. 2. Theoretical blanking force curve [3].

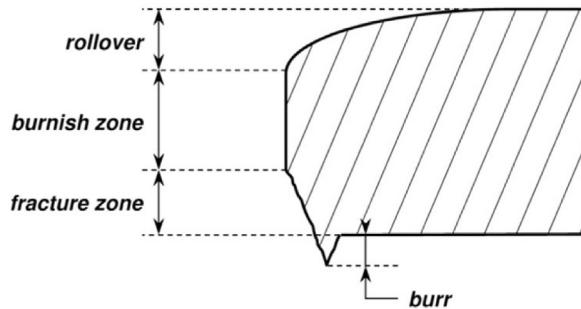


Fig. 3. Typical blanking edge profile [10].

models, are coupled with the material plasticity, where a damage variable is involved in the plastic yielding function. In the uncoupled model approach, the damage variable is not involved in the plasticity yielding function. Instead, a fracture criterion, dependent on the loading history and strain path, is defined, and the element is considered completely damaged when this criterion exceeds a certain threshold. Rice and Tracey [16] criterion, Cockcroft and Latham [17] criterion and Modified Mohr Coulomb criterion [18] are uncoupled fracture criteria widely used in numerical simulations of metal forming. A detailed description of these fracture criteria and their use in metal forming simulation is provided in Tekkaya et al. [19]. In addition to ductile fracture criteria, several other computational aspects must be considered for blanking operations. As blanking operations induce large deformation in sheet metal, numerical problems related to severe element distortions may arise when using a Lagrangian mesh. This problem can be solved by using an adaptive meshing technique that frequently updates the mesh, as it has been shown by Rachik et al. [20].

Although the numerical simulation of the blanking process has been extensively studied in recent years and used in many applications, previous research has only focused on the simulation of the punching (cutting) phase (cf Fig. 2) overlooking simulations for the push and stripping phases, both of which are very important phases that are highly correlated to punch wear, as per Kubik et al. [2]. Therefore, the primary objective of this study is to achieve a highly accurate prediction of the whole blanking force curve using a numerical simulation model that includes the punching phase, the push phase and the stripping phase.

Future work focusing on the development of a tool wear monitoring system that is based on artificial intelligent algorithms will benefit from the numerical simulation procedure outlined in this study. In fact, this numerical procedure will be used to generate numerical data intended to enrich experimental data set for the training of machine learning models. The main advantage of this addition is to explore configurations that are difficult to test experimentally and add them to the training phase of the machine learning model to increase its performance.

In this work, a novel finite element simulation procedure that captures the complete blanking cycle, including the punching phase, sheet metal springback, push phase, and stripping phase is proposed. The simulation result is a full blanking force curve that predicts the force of the punch, push, and withdraw phases (cf Fig. 2). The developed finite element model uses ABAQUS/Explicit® code to simulate the punching phase and ABAQUS/Standard® code for all remaining phases. As an application of this numerical procedure, the influence of the blanking clearance on the full blanking curve (punching-push-stripping forces) and the cut edge profile will be investigated and results will be compared to literature results.

This paper is structured as follows: in Section 2, we present the blanking process parameters and finite element model. In Section 3, we discuss in detail the numerical aspects and parameters used to build this numerical procedure. Section 4 presents the numerical blanking force curve obtained by this procedure, and the results associated with the influence of blanking clearance on the blanking outcome (punch force curve and cut edge) will be shown and discussed. Lastly, a conclusion and a roadmap for future work is given in Section 5.

## 2. Finite element modelling of the blanking process

### 2.1. Sheet metal material behavior modelling

The blanked material is a Dual Phase steel DP600 produced by ArcelorMittal® and mainly used in the automotive industry. Habibi et al. [21] studied many failure criteria on a 1 mm thick DP600 sheet, knowing that the same sheet metal thickness is considered in this work, all mechanical properties and material constitutive law will be collected from their work. The DP600 mechanical properties are shown in Table 1.

The sheet metal elastoplastic behavior is described using a J2-plasticity model with isotropic hardening. Habibi et al. [21] fitted a Hollomon power law to experimental data to characterize the isotropic strain hardening of the DP600 sheet. The Hollomon power law is one of the most popular empirical equations used to describe the stress-strain behavior in work hardening and is expressed as shown in (Eq. (1)).

$$\sigma = K_H * \epsilon_p^n \quad (1)$$

where  $\sigma$  denotes the flow stress,  $\epsilon_p$  denotes the plastic strain,  $K_H$  denotes the Hollomon strength coefficient and  $n$  denotes the strain hardening exponent.

However, the Hollomon equation was found to be too simplistic to describe large plastic strain. Swift [22] proposed another power-law equation expressed as shown in (Eq. (2)).

$$\sigma = K * (\epsilon_p + \epsilon_0)^n \quad (2)$$

where  $\sigma$  denotes the flow stress,  $\epsilon_p$  denotes the plastic strain,  $\epsilon_0$  denotes a pre-strain parameter,  $K$  denotes the strength coefficient and  $n$  denotes the strain hardening exponent.

In this study, the Swift power law will be used to describe the plastic behavior of the DP600 sheet metal, thus the Hollomon strain hardening curve provided in Ref. [21] has been transformed to a Swift law by shifting it so that the curve begins at a flow stress that equals the yielding strength of the material. The resulting Swift hardening curve is shown in Fig. 4 and its parameters are summarized in Table 2.

To model the damage behavior and rupture of the sheet metal, a failure criterion needs to be incorporated into the above-described elasto-plastic behavior. As discussed in Section 1, there are numerous failure criteria available in the literature. According to Tekkaya et al. [19], uncoupled fracture criteria are highly popular in the metal forming community due to their simple implementation and their ability to avoid convergence issues.

In this work, the Modified Mohr Coulomb (denoted MMC3) fracture criteria calibrated for a 1 mm thick DP600 sheet metal by Habibi et al. [21] is used to model the fracture of the sheet metal. The MMC3 criteria is expressed as shown in (Eq. (3)).

$$\bar{\epsilon}_f = \left\{ \frac{K}{C_2} \left[ C_3 + \frac{\sqrt{3}}{2 - \sqrt{3}} (1 - C_3) \left( \left( \sqrt{\frac{3 + \mu^2}{3}} \right) - 1 \right) \right] \times \left[ \sqrt{\frac{1 + C_1^2}{3 + \mu^2}} + C_1 \left( \eta + \frac{1}{3} \left( \frac{-\mu}{\sqrt{3 + \mu^2}} \right) \right) \right] \right\}^{-\frac{1}{n}} \quad (3)$$

where  $\bar{\epsilon}_f$  denotes the equivalent plastic strain at fracture,  $K$  and  $n$  denote respectively the strength coefficient and the strain hardening exponent in the Swift hardening law,  $\mu$  and  $\eta$  denote respectively the Lode parameter and the stress triaxiality and  $[C_1, C_2, C_3]$  represent three parameters to be calibrated using test results.

The Lode parameter and the stress triaxiality factor are two parameters that characterize the stress state.  $[\sigma]$  being the stress tensor, the stress triaxiality is defined as shown in (Eq. (4)).

$$\eta = \frac{\bar{\sigma}}{\sigma_m} \quad (4)$$

$\sigma_m$  is the hydrostatic stress defined by  $\sigma_m = \frac{1}{3} \text{tr}([\sigma])$ .

$\bar{\sigma}$  is the von Mises stress defined by  $\bar{\sigma} = \sqrt{\frac{3}{2} [S] : [S]}$  where  $[S]$  denotes the deviatoric stress tensor defined by  $[S] = [\sigma] - \sigma_m * [I]$ .

For plane stress conditions,  $\mu$  and  $\eta$  are linked by the relationship expressed in (Eq. (5)).

$$\cos \left[ \frac{\pi}{2} \left( 1 - \frac{6}{\pi} \sin^{-1} \left( \frac{-\mu}{\sqrt{\mu^2 + 3}} \right) \right) \right] = \frac{-27}{2} \eta \left( \eta^2 - \frac{1}{3} \right) \quad (5)$$

Habibi et al. [21] calibrated the MMC3 fracture criteria for a 1 mm thick DP600 steel sheet metal using experimental results and

**Table 1**

Mechanical Properties of DP600 steel sheet.

Young's Modulus $E$ (GPa)	Yield Strength $R_{p0.2}$ (MPa)	Tensile Strength $R_m$ (MPa)	Poisson's ratio $\nu$
210	366	700	0.3

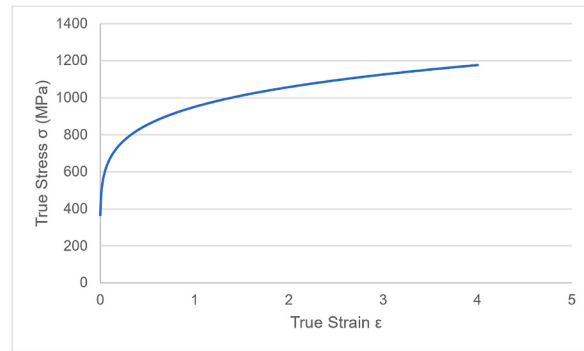


Fig. 4. DP600 sheet metal strain hardening curve.

**Table 2**  
Swift Law parameters values.

$K$ (MPa)	$\epsilon_0$	$n$
950.459	0.002036	0.154

found the values for the above  $[C_1, C_2, C_3]$  parameters shown in Table 3.

The fracture locus ( $\bar{\epsilon}_f$  as a function of  $\eta$ ) associated to the calibrated MMC3 criterion for a 1 mm thick DP600 is shown in Fig. 5. In the following, this fracture locus will be implemented in ABAQUS/Explicit® to model the fracture of the sheet metal in the punch phase of a blanking operation.

## 2.2. Finite element model and process parameters

This blanking process modelling study considered a cylindrical punch with a circular cross section. This choice of geometry allows for axisymmetric modeling due to the revolution symmetry, leading to the consideration of only one meridian plane in the model (Fig. 6). The sheet metal thickness was fixed at 1 mm, and the punch diameter was set at 9 mm. Both the punch and die were assumed to have minimal wear, resulting in cutting-edge radii of 0.03 mm.

Four different values of radial blanking clearance (6 %, 9 %, 12 %, and 15 %) were investigated to examine their impact on the outcome of the blanking process. In general, the radial blanking clearance is expressed as a percentage of the sheet metal thickness based on the formula shown in (Eq. (6)).

$$\text{Radial Clearance (\%)} = \frac{R_d - R_p}{e} * 100 \quad (6)$$

Where  $R_d$  is the radius of the die,  $R_p$  the radius of the punch and  $e$  the thickness of the sheet metal.

The influence of lubrication was incorporated numerically through the contact friction coefficient at the tool sheet interfaces, with a friction coefficient of 0.15 being used in this study to represent a medium level of lubrication. These process parameters are summarized in Table 4.

The finite element model is shown in Fig. 7. As previously mentioned, an axisymmetric modelling approach has been adopted in this study. The punch, the die and the blank holder were modeled as rigid (undeformable) analytical bodies while the only deformable part was the blanked sheet. This assumption was motivated by the fact that, in industrial blanking applications, these blanking tools are made of high-alloyed steels or carbide steels whose hardness is much higher compared to the hardness of the sheet metal material, as discussed by Högman [23]. For the meshing of the sheet metal, a very fine structured mesh has been applied in the shearing region to increase the precision of the obtained results while a coarse one has been used elsewhere to reduce simulation computational cost with a smooth transition mesh built between these meshes. The shearing zone was meshed using CAX4R axisymmetric quadrilateral reduced integration elements while a mixed quadrilateral-based meshing (CAX4R and CAX3 elements) has been employed elsewhere. Coming to the boundary conditions, the die and the blank holder were given fixed constraints while the punch is given a displacement profile to perform the blanking operation. In the punching and push phase, the punch is given a downward displacement while in the stripping phase it is given an upward displacement to withdraw the punch from the die. The value of the punch penetration in the

**Table 3**  
MMC3 calibrated parameters for a 1 mm DP600 sheet metal [21].

$C_1$	$C_2$ (MPa)	$C_3$
0.02	465.07	0.97

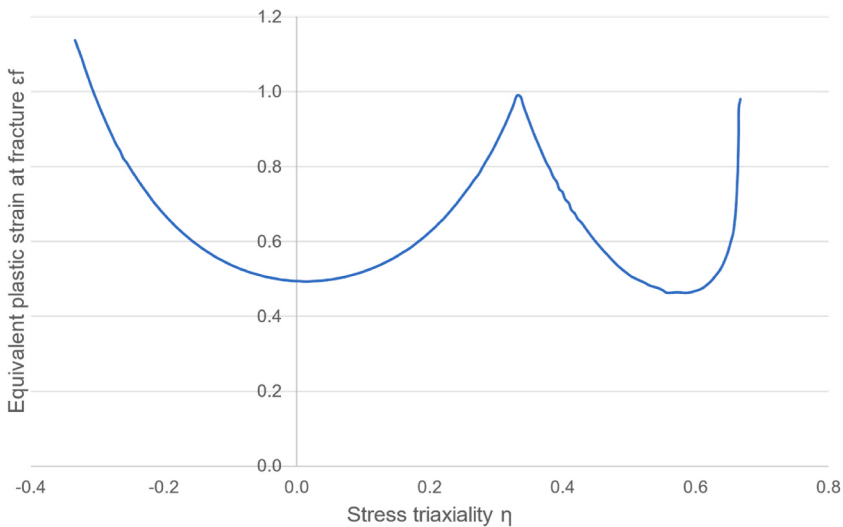


Fig. 5. Fracture locus associated to a MMC3 for a 1 mm DP600 sheet metal.

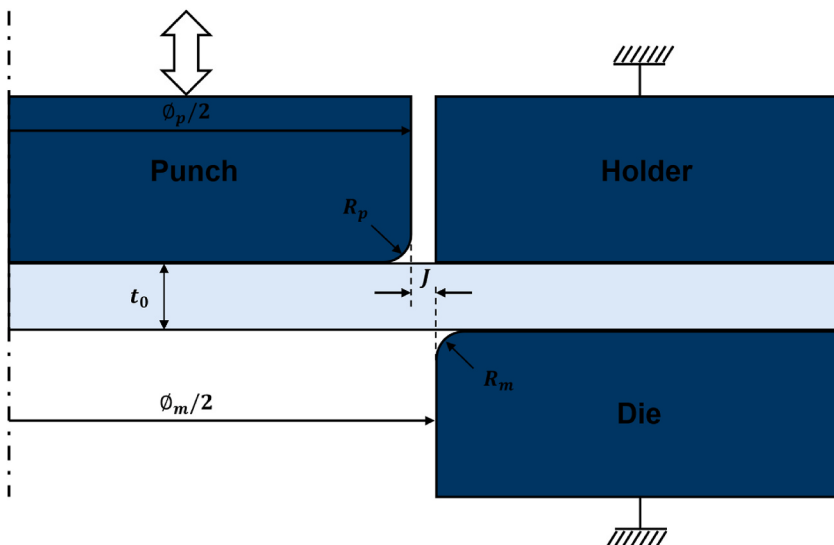


Fig. 6. Axisymmetric blanking simulation scheme.

**Table 4**  
Process parameters.

Sheet thickness (mm)	Punch diameter (mm)	Cutting-edge radii (mm)	Radial Clearance (%)	Friction coefficient
1	9	0.03	6 %, 9 % 12 %, 15 %	0.15

punching phase has been determined based on experimental results and its penetration in the die during the push phase equals the sheet metal thickness. To improve the accuracy and the efficiency of the calculations, smooth punch displacement profiles have been applied. Table 5 summarizes the part properties for this simulation model.

### 3. Numerical simulation methodology

The numerical simulation procedure was conducted using ABAQUS® 2021 package, adopting the large deformation theory and a quasi-static approach. The procedure involved four sequential calculations: punching phase, sheet springback, push phase, and stripping phase. Explicit or implicit solvers (ABAQUS/Explicit®, ABAQUS/Implicit®) were used for each calculation. The punching

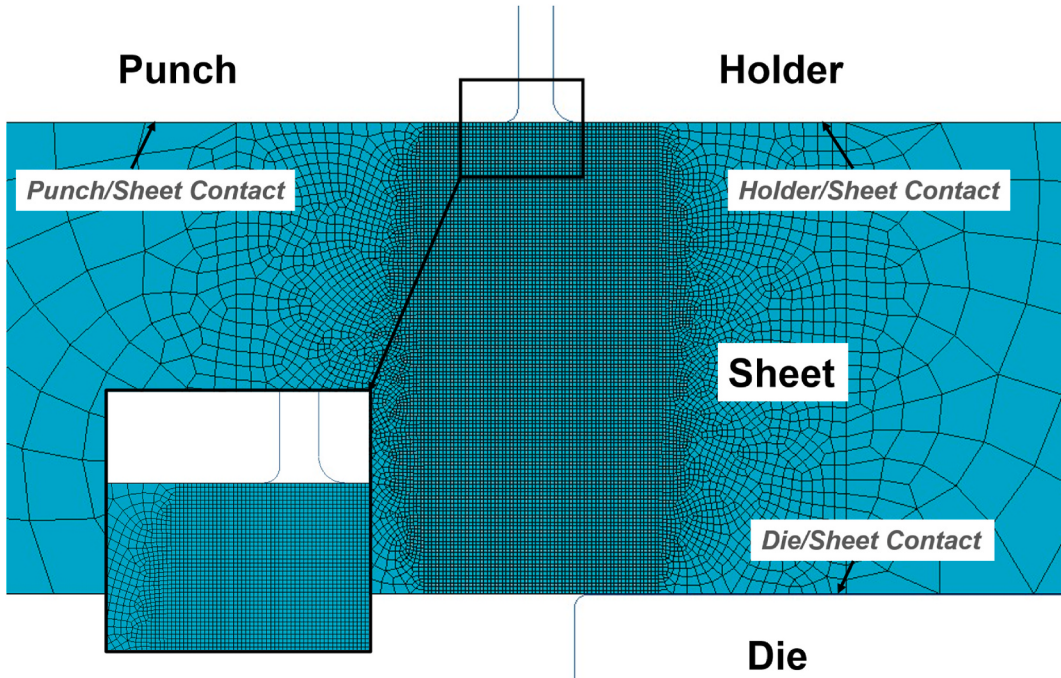


**Fig. 7.** FE model used in the blanking numerical simulation.

**Table 5**

Numerical model part properties.

Name of Part	Kind of part	Number of Nodes	Number of Elements
Punch	Analytical Rigid	–	–
Holder	Analytical Rigid	–	–
Sheet	Deformable	12339	12257
Die	Analytical Rigid	–	–

phase calculation includes highly nonlinear aspects, such as plasticity, sheet metal rupture, and significant deformation of meshing elements. ABAQUS/Explicit® was chosen for this calculation due to its capability to handle such nonlinear problems and for its ALE adaptive remeshing feature, which is crucial for minimizing element distortion and ensuring the convergence of the calculation. In contrast, the remaining three calculations exhibited relatively lower nonlinear characteristics as mesh deformation, plastic loading, and sheet rupture were not involved. These calculations primarily focused on managing the contacts between different components (Fig. 7) while applying a punch displacement to either evacuate the blank or withdraw the punch. Therefore, ABAQUS/Implicit® solver was used for these calculations. In addition, the explicit solver is unable to capture sheet metal spring back.

The four calculations in this procedure were performed sequentially, where the results of the previous calculation served as the starting point for the current one. To accomplish this, the “Predefined Field - Initial State” functionality in ABAQUS® was utilized. This feature facilitates the establishment of an initial state for the sheet metal by exporting all computed fields and states from the preceding

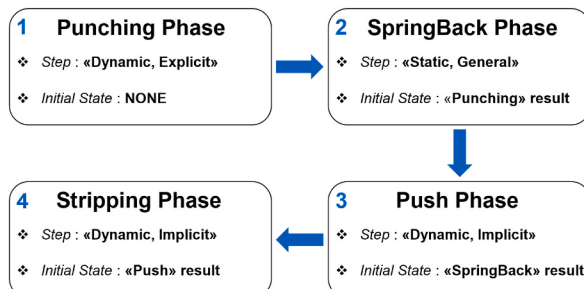


**Fig. 8.** Numerical simulation procedure steps in ABAQUS/CAE®.

calculation and designating them as initial fields for the ongoing one. As a result, this feature establishes a seamless connection between the four calculations, enabling a fully numerical blanking procedure that closely and accurately describes the actual physical process. Fig. 8 provides a comprehensive overview and visualization of the implemented numerical blanking procedure.

The punching phase calculation starts when the punch makes contact with the sheet, marking the beginning of its penetration, and ends when the sheet is completely fractured. This is followed by the calculation of the springback phase, which is maintained until the contact pressure between the sheet and the edges of the punch and die no longer varies. Then the push phase calculation begins and the punch begins to penetrate in the die until it reaches a die penetration equal to the sheet thickness. Once this calculation is completed, the final stripping phase is activated, and the punch begins to withdraw from the die until it returns to its initial position.

It is important to mention the parameters that were used in the explicit solver of the punching phase which is acknowledged as being the most nonlinear phase of this simulation procedure. These parameters were crucial to ensure both the stability and the convergence of this calculation. First, the explicit step was performed with a step time of 0.1 s. Since the numerical model has no time dependence, the value of the step time doesn't affect the final result. A common practice consists on choosing a small value for the step time to speed up the calculation, but this choice should be made carefully as the step time must be consistent with the mass scaling parameter to limit kinetic energy effects. In this work, mass scaling was used through the definition of a target time increment of  $5 \times 10^{-8}$  s. Finally, to avoid element distortion due to large deformation in the shearing region, a Lagrangian-Eulerian adaptive meshing technique (ALE) was used in this numerical calculation with a remeshing sweeps per increment equal to 3 and a frequency equal to 5.

The numerical models incorporated the mechanical properties of the sheet described in Section 2 using a J2-plasticity model with isotropic hardening. The effect of strain rate was not taken into account. The fracture locus obtained from the calibration of an MMC3 model (Section 2) was incorporated in ABAQUS® using a predefined damage initiation criterion called Ductile Damage criterion which is mostly used for ductile metals. This criterion takes as input a fracture locus in a tabular format, so the MMC3 model introduced in Section 2 was discretized and added in that specific format. The Ductile Damage Criterion relies on the accumulation of equivalent plastic strain during the step calculation. A damage state variable  $D$  is calculated for each element of the mesh at each increment of the calculation based on the formula shown in (Eq. (7)).

$$D = \int \frac{d\bar{\epsilon}_p}{\bar{\epsilon}_f(\eta)} \quad (7)$$

where  $D$  is the damage state variable,  $\bar{\epsilon}_p$  the equivalent plastic strain and  $\bar{\epsilon}_f(\eta)$  the equivalent plastic strain at fracture which is none other than the fracture locus given as input. When the damage variable  $D$  of an element reaches the value of unity, the failure criterion is met. To simulate crack propagation, the element deletion option was employed in this work, causing any element that meets the failure criterion to be removed from the mesh.

For handling contact between components, the Abaqus penalty contact algorithm was used. The rigid profiles, including the punch, die, and holder, were defined as the master surfaces, while the boundaries of the sheet metal acted as slave surfaces. A "Hard Contact" normal behavior was specified, and a Coulomb law formulation was used to model the friction between these surfaces.

#### 4. Numerical results and discussion

##### 4.1. Complete blanking force curve and cut edge profile

Using the numerical simulation methodology outlined in Section 3, a series of four simulations corresponding to the four radial clearances described in Section 2.2 were conducted. The resulting blanking force curve for the blanking cycle with a radial clearance of

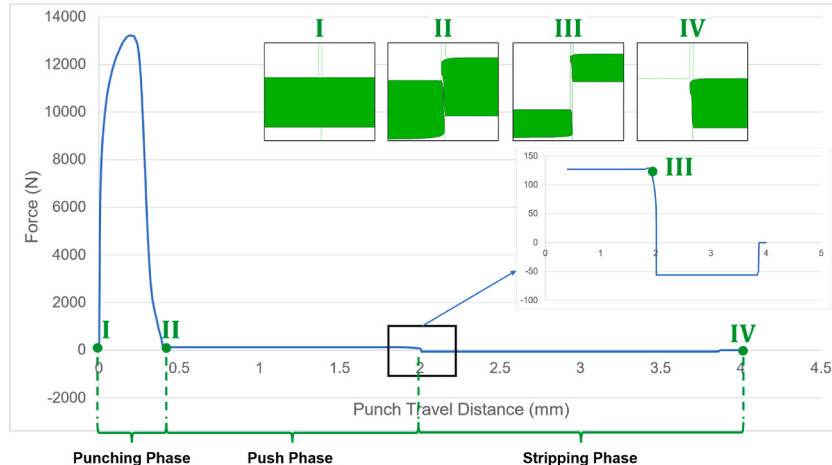


Fig. 9. Complete blanking force curve - radial clearance = 6 %.

6 % is shown in Fig. 9. Additionally, this figure visually depicts the punch position and the corresponding state of the sheet metal at four distinct time points during the cycle.

The comparison of the numerically obtained blanking force curve with the theoretical curve previously discussed in Section 1 reveals a remarkable similarity in shape. The curve clearly exhibits the three primary phases of a blanking process with a punching force that significantly exceeds the pushing and stripping forces. The numerical push and stripping forces are found to be constant throughout the phases. While experimental results may not exhibit this constant behavior, the constancy observed in the numerical results can be attributed to the implementation of a simplified Coulomb friction model for simulating the contact behavior within the finite element (FE) model.

The numerical analysis reveals that the push force during the blanking process is higher than the stripping force, which aligns with the underlying physical principles governing the process. In blanking, the push phase ensures the removal of the blank from the die, while the stripping phase involves the withdrawal of the punch from the die. During the push phase, the forces developed in the punch counteract the friction forces generated between the punch and the cut edge, as well as between the die and the cut blank. On the other hand, the stripping force solely corresponds to the friction forces arising from the interaction between the punch and the cut edge. As a result, the stripping force typically exhibits a lower magnitude compared to the push forces, as the latter also compensates for the additional friction forces associated with the contact between the die and the cut blank.

The advantage of the developed simulation model over existing work lies in its ability to predict the punch force during all the phases of a blanking operation, especially in the push and stripping phases. As per the knowledge of the authors, no previous work has been done to predict the blanking force during these two phases. Predicting an accurate blanking force curve using numerical FE model (Fig. 9) holds pivotal significance in the optimization of the blanking process across multiple dimensions. First, finding the maximum punching force from the curve helps in designing the cutting tool and sensors and reflects the press's capability to successfully execute the cutting operation. Furthermore, various other attributes, prominently influenced by cutting tool wear, can serve as indicative measures for monitoring the cutting tool's wear condition. Notable examples include the punch penetration at fracture, the push force and the stripping force.

Finally, Fig. 10 shows the predicted cut edge profile (Fig. 10-a) and the macrograph of a typical cut edge profile obtained by electron microscopy scanning (Fig. 10-b). A comparative analysis of these two cut edge profiles shows that the numerical simulation procedure developed in this paper is able to capture all the cut edge zones (i.e. Roll over, burnish, fracture and burr). (cf Fig. 3). It should be noted that the predicted cut edge and the macrograph shown in Fig. 10 correspond to different blanking tests. Therefore, this comparison is only qualitative and experimental validation of the model's ability to predict accurate cut edge profiles is provided in the next section.

From an industrial perspective, the precision of the numerical model in predicting an exact cut edge profile is essential. This importance stems from the fact that the dimensional attributes of the distinct zones within a cut edge profile, especially the burr size, unequivocally reflects the quality of the blanking operation. Moreover, tool wear and cut edge quality are highly correlated as this aspect has been investigated by Refs. [2,7]. Consequently, the cut edge profile may serve as a potential parameter for monitoring the wear state of the cutting tool.

In the next section, these zones will be analyzed for the chosen radial clearance values to investigate the influence of radial clearance on the characteristics of the cut edge profile.

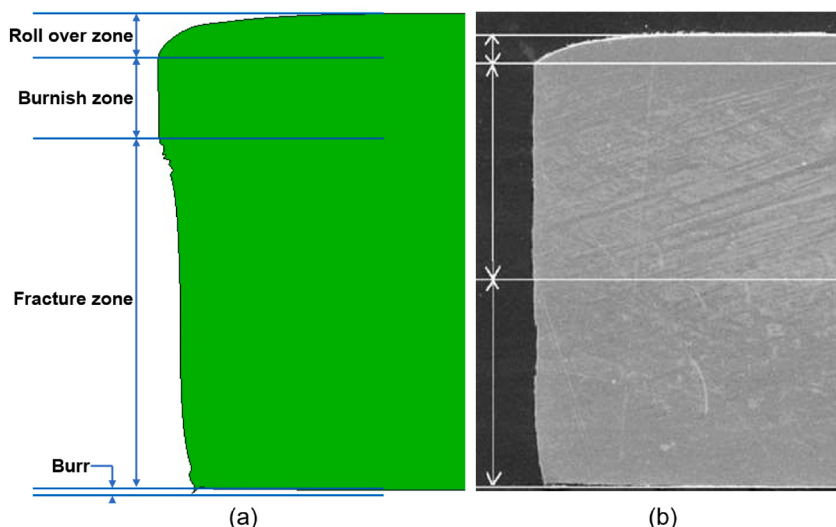


**Fig. 10.** Cut edge profile (a) by FE simulations (b) by scanning electron microscopy analysis [7].

#### 4.2. Effect of clearance on force curve and cut edge quality

This section presents an analysis of the blanking force curves and the properties of the cut edge profiles obtained for the four simulations conducted at different radial clearance values to evaluate the impact of radial blanking clearance on the outcome of the blanking simulation. Fig. 11 illustrates the four blanking force curves obtained for the corresponding radial clearances examined in this study.

The findings in Fig. 11 indicate that as the radial clearance increases, the maximum blanking force (Fig. 11 - a) decreases while the punch displacement until sheet metal rupture (Fig. 11 - b) shows an increasing trend. When the clearance between the punch and the die is increased, more material can undergo plastic deformation in the sheared region. As a result, less shear effort is required to induce rupture in the sheet metal, leading to a decrease in punch force and an increase in punch penetration until rupture (delay of the crack initiation). Fang et al. [5] investigated the effect of the blanking clearance on the force curve and obtained similar results.

However, it is worth noting that the effect of clearance on the maximum blanking force is relatively negligible, with only a 2.18 % decrease observed within a radial clearance range spanning from 6 % to 12 %.

Fig. 11-c illustrates the push and stripping forces corresponding to the four radial clearance values investigated in this study. Both forces exhibit a decreasing trend in magnitude as the radial clearance increases: the push force decreases by 77.7 % and the stripping force decreases by 73.2 % within a radial clearance range spanning from 6 % to 12 %. This observation can be attributed to the interplay between shear stresses, plastic strain, and strain hardening in the shearing region. Specifically, a decrease in radial clearance results in higher shear stresses, leading to increased plastic strain and enhanced strain hardening in the sheet metal material within this region. The increased strain hardening subsequently exerts greater pressure on the punch and die flanks from the cut edge material. Consequently, higher friction forces develop between the punch/sheet metal cut edge and the die/sheet metal cut edge during the push and stripping phases. Therefore, a decrease in radial clearance necessitates higher push and stripping forces to overcome these increased friction forces.

Fig. 12 presents a comparison between the numerically obtained dimensions of different cut edge zones (cf. Fig. 10) in this study and the experimental zone dimensions from a previous investigation conducted by the CETIM - Technical Center of Mechanical Industries. It shows a significant influence of the blanking clearance on the dimensions of these zones and a very good alignment between the numerical trends and the experimental ones. Indeed, the maximum numerical prediction errors of the three zone dimensions are summarized below:

- Fracture zone: A maximum error of 4 % at a 12 % clearance.
- Burnish zone: A maximum error of 14.6 % at a 6 % clearance.
- Roll Over Zone: A maximum error of 12.3 % at a 12 % clearance.

The increasing trends of the roll over and burnish zone as well as the decreasing trend of the fracture zone were expected. Increasing the blanking clearance amplifies the bending effect of the sheet metal material between the punch and the die, resulting in a larger roll-over zone dimension. Additionally, a higher blanking clearance induces more plastic flow of the material in the sheared region. As a result, the crack initiation is delayed leading to a larger burnish zone and a smaller fracture zone.

Furthermore, it should be noted that the previously illustrated increase in punch penetration until rupture (Fig. 11-b) is consistent with the trends observed in the zone dimensions, knowing that the punch penetration until rupture corresponds to the sum of the dimensions of the roll-over and burnish zones.

The investigation of the final hole diameter and the fracture angle, defined as the angle at which fracture occurred in the fracture zone relative to the vertical axis, was conducted for various blanking clearances. These results are presented in Fig. 13.

It can be deduced from Fig. 13(a) that the hole diameter increased by 0.02 % when the clearance increases from 6 % to 12 %. The observed increasing trend of the hole diameter curve with respect to the blanking clearance (Fig. 13 - a) can be attributed to the variation in strain hardening caused by the blanking clearance. As previously explained, a smaller clearance leads to higher levels of strain hardening in the sheet metal material. Consequently, after the punch is withdrawn from the die, the material near the cut edge undergoes greater shrinkage, resulting in a smaller hole diameter.

Coming to the fracture angle, a significant increase of 53 % within a radial clearance range spanning from 6 % to 12 % is shown in Fig. 13-b. In a typical blanking operation, cracks in the sheet metal tend to initiate at the cutting edges and propagate along a straight-line connecting the cutting edges of both the punch and the die. When blanking is performed with a higher clearance, it results in an increased radial distance between the punch and the die, as well as a higher punch penetration until failure, as previously explained. These increased distances will induce a higher fracture angle at the fracture zone. Husson et al. [7] found a similar trend also using numerical simulation.

## 5. Conclusion

This paper introduces a novel FE simulation procedure for modeling the complete blanking operation cycle in the ABAQUS/CAE® 2021 environment. The simulation approach is based on a quasi-static axisymmetric methodology, using both ABAQUS/Explicit® and ABAQUS/Implicit® codes. The behavior of the sheet metal material is characterized using an elasto-plastic Mises constitutive law, incorporating a Modified Mohr Coulomb fracture criterion to predict sheet metal rupture. By employing this procedure, a comprehensive numerical blanking force curve including blanking cycle phases was obtained. Furthermore, the influence of the blanking clearance was investigated. The results clearly demonstrate the significant impact of the blanking clearance on the outcome of the

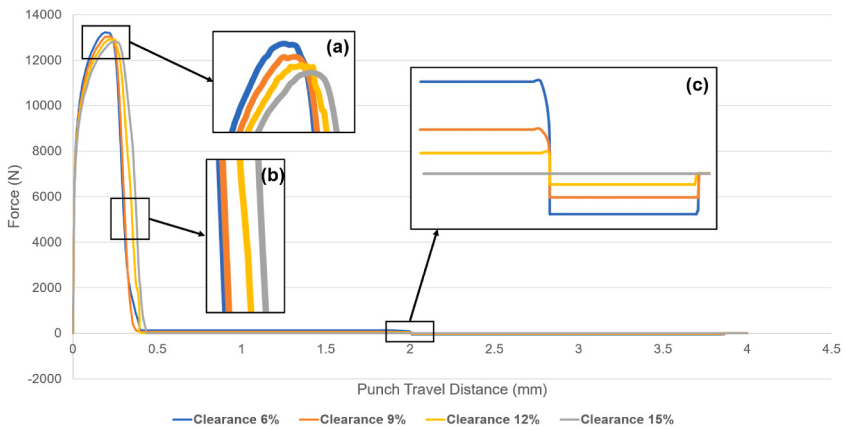


**Fig. 11.** Complete blanking force curve for 6 %, 9 %, 12 % and 15 % radial blanking clearances.

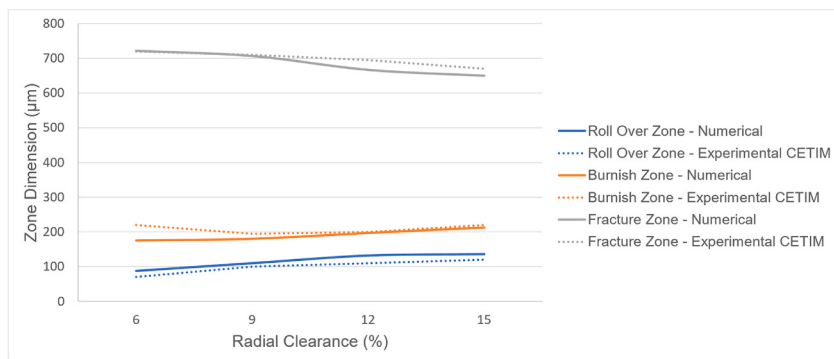


**Fig. 12.** Numerical vs Experimental cut edge zones dimensions comparison.

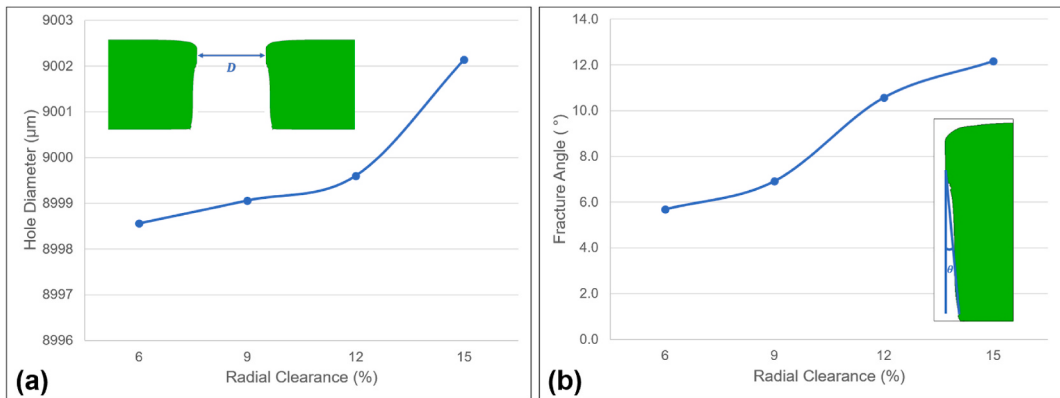


**Fig. 13.** Cut edge profile properties (numerical results) as a function of radial clearance a) Hole Diameter b)Fracture Angle.

blanking operation, including the blanking force curve and the cut edge profile. Importantly, these findings align with previous studies and experimental results.

This innovative procedure offers valuable insights into assessing the influence of process parameters on the outcome of the blanking operation. It provides a means to optimize the quality of the blanked part by fine-tuning process parameters.

#### Ethics approval and consent to participate

Not applicable.

## Consent for publication

Not applicable.

## Data availability

Data will be made available upon request.

## CRediT authorship contribution statement

**Jean Rizk:** Writing – review & editing, Writing – original draft, Validation, Project administration, Methodology, Investigation, Conceptualization. **Mohamed Rachik:** Writing – review & editing, Supervision, Software, Resources. **Andre Maillard:** Writing – review & editing, Supervision, Project administration, Funding acquisition.

## Declaration of competing interest

The authors declare that they have no known competing financial interests or personal relationships that could have appeared to influence the work reported in this paper.

## Acknowledgement

This research was part of a PhD project funded by the CETIM – Technical Center of Mechanical Industries. Hence, the authors would like to thank the CETIM for providing financial support to conduct this study. The authors are also grateful to Roberval Laboratory of UTC – University of Technology of Compiegne for providing numerical calculation facilities to successfully accomplish this work.

## References

- [1] T. Bergs, P. Niemietz, T. Kaufman, D.s.l. Trauth, Punch-to-punch variations in stamping processes: 18th World Symposium on Applied Machine Intelligence and Informatics (Sami), 2020, <https://doi.org/10.1109/SAMI48414.2020.9108761>.
- [2] C. Kubik, J. Hohmann, P. Groche, Exploitation of force displacement curves in blanking—feature engineering beyond defect detection, *Int. J. Adv. Manuf. Technol.* 113 (2021) 261–278, <https://doi.org/10.1007/s00170-020-06450-z>.
- [3] C. Kubik, S.M. Knauer, P. Groche, Smart sheet metal forming: importance of data acquisition, preprocessing and transformation on the performance of a multiclass support vector machine for predicting wear states during blanking, *J. Intell. Manuf.* 33 (1) (2022) 259–282, <https://doi.org/10.1007/s10845-021-01789-w>.
- [4] P. Niemietz, M.J. Kornely, D. Trauth, T. Bergs, Relating wear stages in sheet metal forming based on short-and long-term force signal variations, *J. Intell. Manuf.* 33 (7) (2022) 2143–2155, <https://doi.org/10.1007/s10845-022-01979-0>.
- [5] G. Fang, P. Zeng, L. Lou, Finite element simulation of the effect of clearance on the forming quality in the blanking process, *J. Mater. Process. Technol.* 122 (2–3) (2002) 249–254, [https://doi.org/10.1016/S0924-0136\(02\)00056-0](https://doi.org/10.1016/S0924-0136(02)00056-0).
- [6] R. Hamblin, Blanking tool wear modeling using the finite element method, *Int. J. Mach. Tool Manufact.* 41 (12) (2001) 1815–1829, [https://doi.org/10.1016/S0890-6955\(01\)00024-4](https://doi.org/10.1016/S0890-6955(01)00024-4).
- [7] C. Husson, J.P.M. Correia, L. Daridon, S. Ahzi, Finite elements simulations of thin copper sheets blanking: Study of blanking parameters on sheared edge quality, *J. Mater. Process. Technol.* 199 (1–3) (2008) 74–83, <https://doi.org/10.1016/j.jmatprotec.2007.08.034>.
- [8] A. Totre, R. Nishad, S. Bodke, An overview of factors affecting in blanking processes, *International Journal of Emerging Technology and Advanced Engineering (IJETAE)* 3 (3) (2013) 390–395.
- [9] S.K. Maiti, A.A. Ambekar, U.P. Singh, P.P. Date, K. Narasimhan, Assessment of influence of some process parameters on sheet metal blanking, *J. Mater. Process. Technol.* 102 (1–3) (2000) 249–256, [https://doi.org/10.1016/S0924-0136\(99\)00486-0](https://doi.org/10.1016/S0924-0136(99)00486-0).
- [10] E. Falconnet, J. Chambert, H. Makich, G. Monteil, Prediction of abrasive punch wear in copper alloy thin sheet blanking, *Wear* 338 (2015) 144–154, <https://doi.org/10.1016/j.wear.2015.06.007>.
- [11] M. Sahli, X. Roizard, G. Colas, M. Assoul, L. Carpenter, P.H. Cornual, J.P. Barbe, Modelling and numerical simulation of steel sheet fine blanking process, *Procedia Manuf.* 50 (2020) 395–400, <https://doi.org/10.1016/j.promfg.2020.08.072>.
- [12] R.K. Pathak, A.R. Kumar, G.K. Ananthasuresh, Simulations and experiments in punching spring-steel devices with sub-millimeter features, *J. Manuf. Process.* 15 (1) (2013) 108–114, <https://doi.org/10.1016/j.jmapro.2012.09.018>.
- [13] Y. Liu, K. Ji, Y. Zhang, Y. Song, F. Yin, Effect of grain size on fine micro-blanking for Inconel 718 foil, *J. Manuf. Process.* 107 (2023) 472–484, <https://doi.org/10.1016/j.jmapro.2023.10.022>.
- [14] A continuous damage mechanics model for ductile fracture, *Lemaitre J* (1985), <https://doi.org/10.1115/1.3225775>.
- [15] Continuum theory of ductile rupture by void nucleation and growth: Part I—Yield criteria and flow rules for porous ductile media, *Gurson A. L* (1977), <https://doi.org/10.1115/1.3443401>.
- [16] J.R. Rice, D.M. Tracey, On the ductile enlargement of voids in triaxial stress fields, *J. Mech. Phys. Solid.* 17 (3) (1969) 201–217, [https://doi.org/10.1016/0022-5096\(69\)90033-7](https://doi.org/10.1016/0022-5096(69)90033-7).
- [17] Latham, M. Cockcroft, etD, Ductility and workability of metals, *J. Inst. Met.* 96 (1968) 33–39.
- [18] Y. Bai, T. Wierzbicki, Application of extended Mohr–Coulomb criterion to ductile fracture, *Int. J. Fract.* 161 (1) (2010) 1–20, <https://doi.org/10.1007/s10704-009-9422-8>.
- [19] A.E. Tekkaya, P.O. Bouchard, S. Bruschi, C.C. Tasan, Damage in metal forming, *CIRP Annals* 69 (2) (2020) 600–623, <https://doi.org/10.1016/j.cirp.2020.05.005>.
- [20] M. Rachik, J.M. Roelandt, A. Maillard, Some phenomenological and computational aspects of sheet metal blanking simulation, *J. Mater. Process. Technol.* 128 (1–3) (2002) 256–265, [https://doi.org/10.1016/S0924-0136\(02\)00460-0](https://doi.org/10.1016/S0924-0136(02)00460-0).
- [21] N. Habibi, A. Ramazani, V. Sundararaghavan, U. Prahl, Failure predictions of DP600 steel sheets using various uncoupled fracture criteria, *Eng. Fract. Mech.* 190 (2018) 367–381, <https://doi.org/10.1016/j.engfracmech.2017.12.022>.
- [22] H. Swift, Plastic instability under plane stress, *J. Mech. Phys. Solid.* 1 (1) (1952) 1–18, [https://doi.org/10.1016/0022-5096\(52\)90002-1](https://doi.org/10.1016/0022-5096(52)90002-1).
- [23] B. Höglund, Karlstad, Sweden, Steel for Press Tools: Blanking of Ultra High Strength Steel Sheet, in: *Proceedings of the 6th International Tooling Conference: the Use of Tool Steels: Experience and Research*, 2002.